NJC

ROYAL SOCIETY OF CHEMISTRY

PAPER

Cite this: *New J. Chem.*, 2023, **47**, 18856

Palladium immobilized on guanidine functionalized magnetic nanoparticles: a highly effective and recoverable catalyst for ultrasound aided Suzuki–Miyaura cross-coupling reactions†

Sumanth Hegde, [a] Aatika Nizam, *[a] Ajesh Vijayan, [a] Ramesh B. Dateer [b] and Suresh Babu Naidu Krishna *[cd]

Received 24th July 2023,
Accepted 15th September 2023

DOI: 10.1039/d3nj03444e

rsc.li/njc

We designed and prepared a palladium catalyst that can be magnetically recyclable by anchoring guanidine moiety on the surface of Fe_3O_4 nanoparticles, named Fe_3O_4@SiO_2-TCT-Gua-Pd. It was established to be a potent catalyst for the Suzuki–Miyaura cross-coupling reaction (SMCR) in the EtOH/H_2O system under ultrasonic conditions. FT-IR spectroscopy, field-emission scanning electron microscopy (FESEM), energy dispersive X-ray (EDX) microanalysis, vibration sample magnetometry (VSM), transmission electron microscopy (TEM), X-ray photoelectron spectroscopy (XPS), thermogravimetric analysis (TGA), and inductively coupled plasma atomic emission spectrometry (ICP-AES) analyses were used to characterize the structure of the Fe_3O_4@SiO_2-TCT-Gua-Pd nanoctalyst. The Fe_3O_4@SiO_2-TCT-Gua-Pd catalyst produced favorable coupled products with excellent yields and was harmonious with various aryl halides and aryl boronic acids. The stability, low palladium leaching, and heterogeneous nature of the nanocatalyst were confirmed by a hot-filtration test. The palladium nanocatalyst could be easily recovered by magnetic field separation and recycled at least 6 times in a row without noticeable loss in its catalytic activity.

1. Introduction

Eco-friendly organic chemical processes are needed in developing the fields of green chemistry[1,2] due to the increase in pollution and its severe effects on ecosystems.[3] One of the steps towards green synthesis has been proven to be the use of ultrasonography. It is fascinating to know that organic transformations can occur in the presence of echoes of ultrasound pulses, and it effectively reduces the reaction times while also increasing the reactivity of chemical reactions.[4,5] Iron oxide nanoparticles, with their distinctive physicochemical properties and diverse uses, have attracted considerable attention in drug delivery, magnetic sensors, magnetic resonance imaging, and magnetic refrigeration.[6] Recently, they have been found to be promising solid support for the immobilization of transition metal nanoparticles for organic transformation.[7,8] The cross coupling between two different trigonal carbons has been considered a potent synthetic procedure, and the Suzuki–Miyaura cross-coupling reaction (SMCR) is one among them with aryl halides and aryl boronic acids as the coupling partners to yield the corresponding biphenyls.[9–12] Biphenyls have wide applications in many fields, such as agrochemicals,[13] pharmaceuticals,[14] natural products, and display industries.[15] SMCR has gained much utility over the last two decades, involving palladium, cobalt, nickel, copper, and iron complexes as catalysts.[16–18]

Despite the prevalence of the reaction, various studies have been conducted recently to develop a stable, economical, and effective heterogenous catalyst using various solid supports, such as carbon-based materials,[19,20] graphene oxides,[21] boehmite,[22] and metal–organic frameworks.[23–25] Iron oxide is one of the utilized supports for anchoring the metal nanoparticles as a catalyst in organic synthesis for its inherent features, such as paramagnetism, ease of synthesis, compatibility with the environment, and easy separation by an external magnet.[26–30] On the other hand, guanidine, a naturally occurring nitrogen-rich compound acting as a superbase and

[a] *Department of Chemistry, CHRIST (Deemed to be University), Bangalore-560029, India. E-mail: sumanth.hegde@res.christuniversity.in, aatika.nizam@christuniversity.in, ajesh.vijayan@christuniversity.in*
[b] *Centre for Nano and Material Sciences, Jain University, Bangalore, Karnataka 562112, India. E-mail: d.ramesh@jainuniversity.ac.in*
[c] *Institute for Water and Wastewater Technology, Durban University of Technology, PO Box 1334, Durban-4000, South Africa. E-mail: sureshk@dut.ac.za*
[d] *Department of Biomedical and Clinical Technology, Durban University of Technology, Durban-4000, South Africa*

† Electronic supplementary information (ESI) available. See DOI: https://doi.org/10.1039/d3nj03444e

N-donor ligand to easily coordinate with the metal ions, is used for the surface functionalization of magnetic supports.[31–33] Owing to these properties, we decided to graft guanidine for the better chelation of palladium ions onto the surface of iron oxide nanoparticles. In the recent past, non-conventional techniques like microwave irradiation, photoactivated reactions, and sunlight and ultrasound-mediated processes have become more popular.[34–37] Among these energy sources, ultrasonication has gained significant attention and has been frequently used in catalysis since it offers low reaction time, mild conditions, high selectivity, and operational ease.[38,39] Sonochemistry uses the influence of an acoustic field; bubbles are generated from the existing gas nuclei in liquids, which in turn oscillate in a nonlinear manner and violently collapse in specific experimental conditions, generating enormous pressure and temperature.[40] As a result, the process of ultrasonication offers enormous potential for the synthesis of organic molecules due to its decreased energy consumption and chemical waste creation.[41] Despite various remarkable advancements in catalyst systems, ultrasound-mediated cross-coupling reactions remain unexplored to that extent. The present study describes an ultrasound-mediated method that provides the efficient and facile synthesis of biphenyls using magnetically recoverable Fe_3O_4@SiO_2-TCT-Gua-Pd nanocatalyst.

2. Materials and methods

All organic materials were commercially procured from Merck (India) and used without purification. Fourier Transform-Infrared spectra were recorded on Shimadzu IR Spirit spectrophotometer, and the XRD pattern was recorded on a Miniflex 600 diffractometer using CuKα radiation in the range of 10°–90° (2 theta). EZ-7 vibrating sample magnetometer was used to assess the magnetic properties. The reactions and purity determination of substrates were monitored by thin-layer chromatography (TLC) on silica-gel plates. The TGA analysis was carried out on an NJA – STA 2500 Regulus simultaneous TGA/DTA analyzer. ICP-AES analysis was carried out on ARCOS, Simultaneous ICP spectrometer with R.F. generator of 27.12 MHz. Proton (^{1}H) and carbon (^{13}C)-NMR were recorded on Bruker instrument at 400 MHz, relative to TMS as external standard.

2.1. Preparation of the catalyst

2.1.1. Synthesis of iron oxide (Fe_3O_4) magnetic nanoparticles (MNPs). MNPs were synthesized according to the well-known co-precipitation method.[42] In brief, $FeCl_3{\cdot}6H_2O$ (5.8 g, 2.1 mmol) and $FeCl_2{\cdot}4H_2O$ (2.1 g, 1.0 mmol) in 100 mL deionized water were ultrasonicated for 30 min followed by heating to 80 °C. Then, 10 mL of 25% aqueous ammonia was added dropwise at the rate of 4 mL min^{-1} under the N_2 atmosphere and stirred for 30 min. The resulting black precipitate was magnetically decanted from the solution, and the obtained solid was repeatedly washed with EtOH and deionized (DI) water to remove any impurities, and it was vacuum dried at 65 °C for 12 h.

2.1.2. Preparation of silica-coated MNPs. Fe_3O_4 nanoparticles (1.0 g) obtained in the previous step were dispersed in 40 mL ethanol and 10 mL deionized water using an ultrasonicator for 30 min, and to this suspension was added 0.5 mL of tetraethyl orthosilicate, followed by the addition of 0.8 mL of aq. NH_4OH and the mixture was stirred at ambient temperature for 12 h. After that, Fe_3O_4@SiO_2 nanoparticles were removed from the reaction mixture with an external magnet, washed with DI water and ethanol, and vacuum dried at 80 °C for 12 h.

2.1.3. Functionalization of Fe_3O_4@SiO_2 MNPs nanoparticles. To 100 mL of dry toluene, approximately 1.0 g of Fe_3O_4@SiO_2 nanoparticles were added and ultrasonicated for 0.5 h, and to this, 3-aminopropyltriethoxysilane (10 mL) was added and stirred for 18 h under nitrogen atmosphere at room temperature. The amine-functionalized solid particles were separated using a magnet, washed, and dried at 65 °C for 24 h.

2.1.4. Synthesis of Fe_3O_4@SiO_2-TCT nanoparticles. To the dispersed solution of Fe_3O_4@SiO_2-NH_2 (0.8 g) in tetrahydrofuran (20 mL), cyanuric chloride (1.0 g) and 0.7 mL of diisopropylethylamine were added under N_2 atmosphere, and the solution was agitated at ambient temperature for 18 h. Then, the synthesized Fe_3O_4@SiO_2-TCT nanoparticles were separated magnetically from the reaction mixture, washed with ethanol, and dried at 70 °C for 4 h.

2.1.5. Synthesis of Fe_3O_4 @ SiO_2-TCT-Gua-Pd nanoparticles. Guanidine hydrochloride (0.7 g) was dissolved in 0.5 g of Fe_3O_4@ SiO_2-TCT nanocomposites dispersed in acetonitrile (30 mL) and vigorously stirred at room temperature. After 6 h, the nanoparticles were magnetically decanted and dried at 75 °C for 5 h after being washed several times with EtOH.[42] Then, the nanocomposite obtained was redispersed in 20 mL ethanol containing 0.04 g of $Pd(OAc)_2$ (0.25 mmol g^{-1}) and stirred at room temperature for 24 h to provide the titled heterogeneous nanocatalyst. The final nanocatalyst was separated from the mixture magnetically, washed repeatedly with EtOH/H_2O, and vacuum dried for 12 h at 60 °C.

2.2. General reaction procedure for Suzuki–Miyaura cross-coupling reaction

The mixture of 1.0 mmol of aryl halides, aryl boronic acid (1.2 mmol), K_2CO_3 (3.0 mmol), and 4 mL of EtOH : water (3 : 1) solution was loaded in a 15 mL vial and purged with N_2 gas. To this mixture, 0.1 mol% of Fe_3O_4@SiO_2-TCT-Gua-Pd was added and sonicated for 20 min at 50 °C. The progress of the reaction was monitored using TLC. After the reaction was complete, the reaction mixture was diluted with ethyl acetate and water. The catalyst was separated at this stage by an external magnet, washed with ethyl acetate, dried, and repeated for subsequent runs under the same conditions. Evaporation of the ethyl acetate layer yielded the crude that was purified by column chromatography with 0–10% ethyl acetate in hexane to afford pure products.

3. Results and discussion

The magnetic nanoparticles were synthesized according to the literature using the salts of iron and aqueous ammonia as a base.[42] The further functionalization was done according to

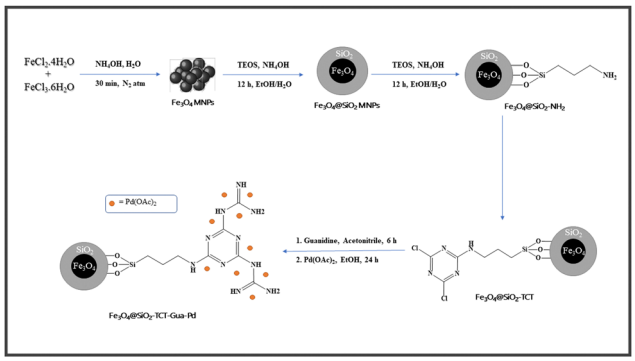

Scheme 1 Preparation of Fe_3O_4@SiO_2-TCT-Gua-Pd nanoparticles.

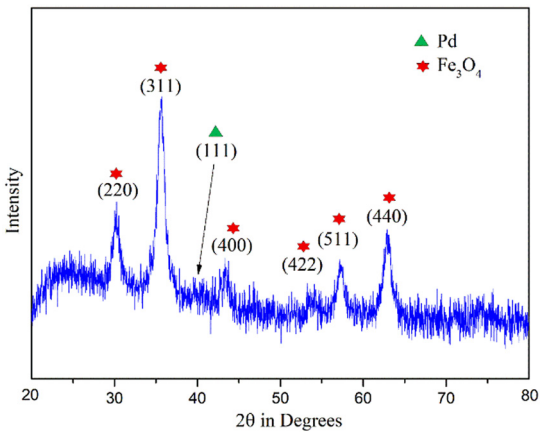

Fig. 2 XRD pattern of Fe_3O_4@SiO_2-TCT-Gua-Pd.

Scheme 1. Finally, palladium incorporation was done by treating with palladium acetate. The palladium content in Fe_3O_4@SiO_2-TCT-Gua-Pd was found to be 2.76 wt% (0.27 mmol g^{-1}) by the ICP-AES analysis. To investigate the structure of the synthesized nanocatalysts, FT-IR, TGA, XRD, FESEM, EDX, TEM, XPS, and VSM analyses were done. The catalytic performance of Fe_3O_4@SiO_2-TCT-Gua-Pd has been investigated towards SMCR between a series of substituted aryl halides and substituted aryl boronic acids.

3.1. Characterization studies

FT-IR analysis. The FT-IR characteristic peak of Fe_3O_4 could be observed at 586 cm^{-1}, which is due to the Fe–O stretching vibrations (Fig. 1a). Further functionalization with TEOS and APTES was confirmed by the appearance of a strong peak near 1057 cm^{-1}, which can be attributed to the stretching vibrations of Si–O–Si bonds (Fig. 1b and c). Simultaneously, the intensity of 586 cm^{-1} reduced due to the uniform coating of silica over Fe_3O_4. The FTIR spectrum of Fe_3O_4@SiO_2-TCT-Gua showed the peaks at 1547 cm^{-1} and 1632 cm^{-1}, corresponding to the stretching of N-C from TCT and a strong peak at 3351 cm^{-1} can be related to NH, NH_2 groups of guanidine (Fig. 1d). Further, the final catalyst showed the 3351 cm^{-1} peak with lesser intensity, which is due the formation of a complex with palladium nanoparticles (Fig. 1e).

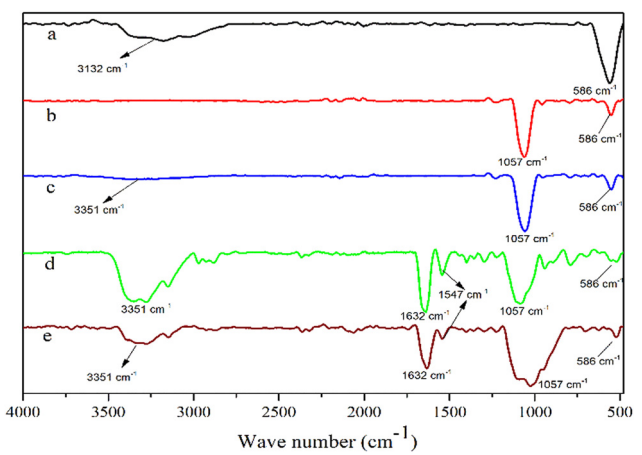

Fig. 1 FTIR spectra of (a) MNPs, (b) Fe_3O_4@SiO_2 NPs, (c) Fe_3O_4@SiO_2-NH_2 NPs, (d) Fe_3O_4@SiO_2-TCT-Gua NPs, and (e) Fe_3O_4@SiO_2-TCT-Gua-Pd nanocatalyst.

XRD analysis. The final catalyst showed peaks from diffraction at 2θ = 30.4°, 35.7°, 43.4°, 53.8°, and 63.0°, corresponding to (2 2 0), (3 1 1), (4 0 0), (4 2 2), (5 1 1) and (4 4 0), which are readily recognized from the XRD pattern, as shown in Fig. 2. This pattern clearly confirms the cubic-phase of Fe_3O_4 MNPs. This demonstrated that MNPs' crystal structure was unaltered, even after modification with silica and guanidine. Also, the weak diffraction peak at 2θ = 39° corresponds to the (1 1 1) plane of the supported palladium. The absence of other palladium peaks clearly shows that it is purely in its amorphous form and spreads over the surface homogeneously. Using the Debye–Scherrer equation, the average crystallite size of the nanocatalyst is determined from XRD data.

$$d = \frac{k\lambda}{\beta \cos\theta}$$

where d is the crystal's particle size, k is the Scherrer constant (0.94), β is the full width at half maximum (FWHM) in radians, λ is the wavelength of the X-ray (0.15406 nm), and θ is the position of the diffraction peak maximum. According to the equation mentioned above and by calculating for all the diffraction peaks of the XRD, the average diameter of the Fe_3O_4@SiO_2-TCT-Gua-Pd nanocatalyst was found to be 16 nm.

FE-SEM and EDS mapping. FE-SEM analysis was used to examine and study the particle size, shape, and surface morphology of the synthesized catalyst. Fig. 3 demonstrates the FE-SEM images of Fe_3O_4@ SiO_2-TCT-Gua-Pd. As shown in Fig. 3, the prepared catalyst presented spherical morphology and relatively uniform size distribution. The spatial distribution and density of atoms in the prepared nanocatalyst were evaluated using elemental mapping. As shown in Fig. 4, Pd distribution is homogenous, along with carbon, oxygen, silicon, nitrogen, and iron in the catalyst. Energy dispersive X-ray (EDX) studies showed the existence of all the elements mentioned earlier, which in turn successfully verifies each step in the catalyst's synthesis. The amount of Pd trapped with the catalyst was detected to be 2.81% by weight. However, this is well

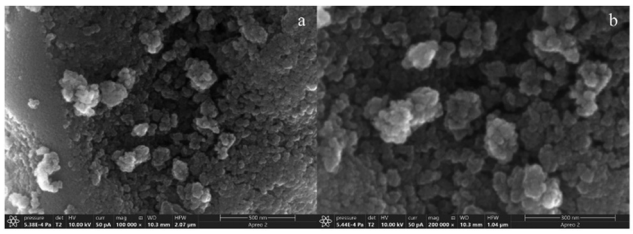

Fig. 3 FE-SEM images of Fe_3O_4@SiO_2-TCT-Gua-Pd nanocatalyst at (a) higher magnification and (b) lower magnification.

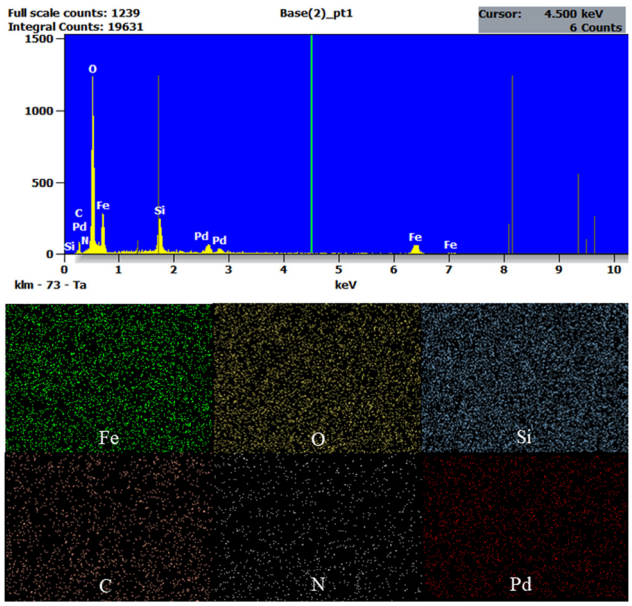

Fig. 4 EDX spectrum and elemental map of iron, oxygen, silicon, carbon, nitrogen, and palladium in the Fe_3O_4@SiO_2-TCT-Gua-Pd catalyst.

matched with ICP-AES analysis, which confirmed the palladium content to be 2.76%.

TEM analysis. The HR-TEM images unveiled the successful coating of amorphous silica on the surface of the MNPs which could be seen as brighter area around the darker core. Due to the magnetic attraction between the nanoparticles, a small assemblage and stacking could be seen (Fig. 5). The average

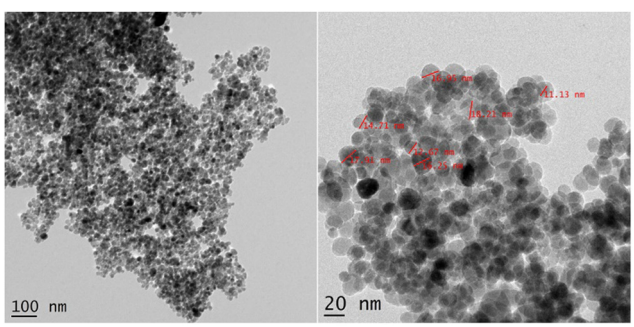

Fig. 5 HR-TEM images of the Fe_3O_4@SiO_2-TCT-Gua-Pd nanocatalyst at different magnifications.

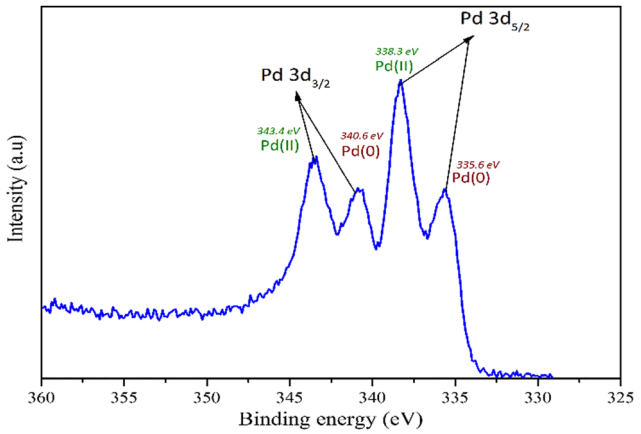

Fig. 6 XPS analysis showing high resolution spectrum of Pd 3d for Fe_3O_4@SiO_2-TCT-Gua-Pd catalyst.

particle size of the nanocatalyst is approximately 15 nm to 20 nm with almost spherical morphology.

XPS analysis. XPS was employed to investigate the oxidation state of Pd species in Fe_3O_4@SiO_2-TCT-Gua-Pd nanocatalyst. The XPS core level spectrum for Pd 3d characterized by spin–orbit splitting is displayed in Fig. 6. The Pd 3d spectrum comprises two main doublets indicating two different Pd states. However, the Pd $3d_{5/2}$ (338.3 eV) along with Pd $3d_{3/2}$ (343.4 eV) of higher binding energies with higher intensity prove that Pd exists in a Pd^{2+} state as single atoms or clusters in the catalyst. Pd(0) state is also observed with binding energies $3d_{5/2}$ (335.6 eV) and Pd $3d_{3/2}$ (340.6 eV), which is due to the reduction at guanidine sites.

Thermogravimetric (TGA) analysis. To examine the thermal stability of the magnetic nanocatalyst and percentage of organic functional groups, thermogravimetric analysis was carried out. The thermogravimetric analysis curve of the nanocatalyst is shown in Fig. 7. The initial 5% weight loss below 210 °C could possibly be due to the loss of physically adsorbed water molecules. Further weight loss observed (15%) at 225–310 °C is mostly caused by the breakdown of grafted organic moieties on the surface of the MNPs. Consequently, it is proven that the nanocatalyst is stable up to 225 °C and can be employed in organic synthesis.

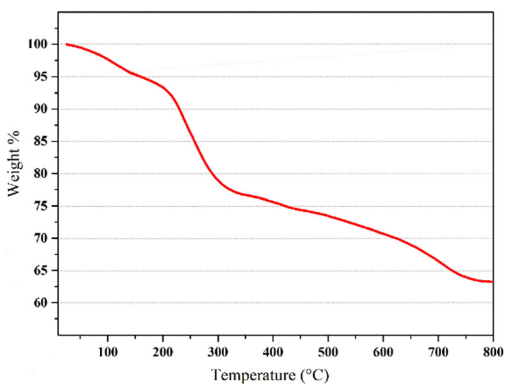

Fig. 7 TGA curve of Fe_3O_4@SiO_2-TCT-Gua-Pd catalyst.

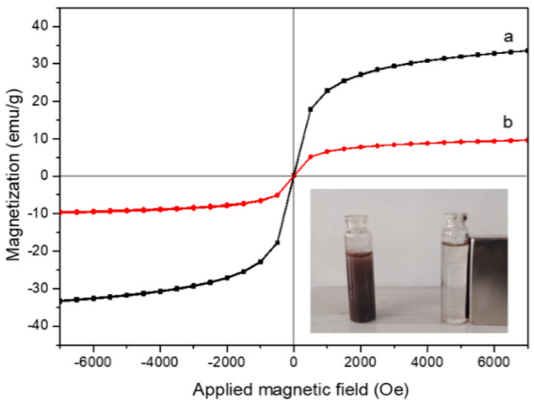

Fig. 8 Magnetization curve of (a) bare Fe_3O_4 nanoparticles and (b) Fe_3O_4@SiO_2-TCT-Gua-Pd nanocatalyst.

Vibrating sample magnetometry (VSM) analysis. Vibrating sample magnetometry analysis was employed to investigate the magnetic properties of the bare MNPs and the Fe_3O_4@SiO_2-TCT-Gua-Pd catalyst. As shown in Fig. 8a, MNPs have a magnetization saturation of 33.4 emu g^{-1} at room temperature; however, it decreases to 10.56 emu g^{-1}. Fig. 8b suggests the coating silica along with the functionalization of TCT and guanidine onto the surface of Fe_3O_4 NPs. It is seen that there is no hysteresis and Fe_3O_4@SiO_2-TCT-Gua-Pd catalyst is superparamagnetic. Even though the magnetization saturation has decreased, the separation of the catalyst from the solution is still effective with the help of an external magnetic field, which is shown in Fig. 8 inset.

3.2. Experiments on catalytic activity

To assess the catalytic efficiency of the Fe_3O_4@SiO_2-TCT-Gua-Pd catalyst for the Suzuki–Miyaura cross-coupling reaction, 4-bromoacetophenone and phenylboronic acid were selected as model coupling partners (Scheme 2), and parameters were varied to optimize the reaction conditions (Table 1).

Catalytic behavior of Fe_3O_4@SiO_2-TCT-Gua-Pd in Suzuki–Miyaura coupling reactions. Possessing the best reaction conditions, a broad range of structurally diverse aryl halides were reacted with aryl boronic acids in the presence of Fe_3O_4@SiO_2-TCT-Gua-Pd catalyst and 3.0 mmol K_2CO_3 with EtOH : H_2O mixture as solvent (Scheme 3) under ultrasonic condition and the results are tabulated in Table 2. To further demonstrate the impact of the ultrasonication process, a model reaction was conducted under conventional heating (50 °C, 4 h), with the results shown in Table 2. All the aryl iodides gave better yields when compared to their corresponding bromide

Table 1 Optimization of Suzuki–Miyaura cross-coupling of 4-bromoacetophenone and phenylboronic acid catalyzed by Fe_3O_4@SiO_2-TCT-Gua-Pd[a]

Entry	Catalyst (mol%)	Base	Solvent	Temp. (°C)	Time (min)	Conversion[b] (%)
1	0.1	Et_3N	DCM	40	60	10
2	0.1	Et_3N	DMF	40	60	25
3	0.1	Et_3N	DMSO	40	60	Trace
4	0.1	K_2CO_3	H_2O	40	40	40
5	0.1	KOH	EtOH : H_2O	40	40	60
6	0.1	K_2CO_3	EtOH : H_2O	40	30	93
7	0.1	NaOAc	EtOH : H_2O	40	30	75
8	0.1	Cs_2CO_3	EtOH : H_2O	40	20	83
9	0.1	K_2CO_3	EtOH : H_2O	30	20	69
10	0.1	K_2CO_3	EtOH : H_2O	40	20	93
11	**0.1**	**K_2CO_3**	**EtOH : H_2O**	**50**	**20**	**98**
12	0.1	K_2CO_3	EtOH : H_2O	60	20	95
13	0.05	K_2CO_3	EtOH : H_2O	50	20	80
14	0.15	K_2CO_3	EtOH : H_2O	50	20	86
15[c]	—	K_2CO_3	EtOH : H_2O	50	20	0
16[d]	0.3	K_2CO_3	EtOH : H_2O	50	20	0

[a] Reaction condition: 1.0 mmol of 4-bromoacetophenone, (1.2 mmol) of phenylboronic acid, (3.0 mmol) of K_2CO_3, Fe_3O_4@SiO_2-TCT-Gua-Pd, 50 °C under ultrasonication. [b] Conversions were determined by thin-layer chromatography. [c] No catalyst was used. [d] Fe_3O_4@SiO_2-NH_2 was used as a catalyst.

and chloride analogues. This is because of the easy cleavage of the Ar–I bond that undergoes oxidative addition with the Pd. The lower yields from aryl chlorides may have been caused by their weak reactivity towards oxidative addition in the catalysis. It is well established that ultrasonication in a heterogeneous medium increases the rate of the reaction through a process called acoustic cavitation.[43–45] Here, it is clear that the implosion through acoustic cavitation activates the catalyst and reactants as compared to conventional heating. When compared to conventional heating, ultrasonication produced a greater yield with a quicker reaction time for the catalyst (entry 18, Table 2). All reactions were carried out on a 1.0 mmol scale, and individual product yields have been tabulated in Table 2.

3.3. Reusability of Fe_3O_4@SiO_2-TCT-Gua-Pd catalyst

One of the most intriguing benefits of this heterogeneous nanocatalyst is its recovery and recyclability. Hence, a recyclability test was also performed for Fe_3O_4@SiO_2-TCT-Gua-Pd nanocatalyst towards SMCR, as shown in Scheme 2. Following the reaction, the nanocatalyst was easily separated from the reaction mixture using an external magnet, washed with ethyl acetate, dried, and then reused in a subsequent run. It was noticed that Fe_3O_4@SiO_2-TCT-Gua-Pd can be easily recycled six

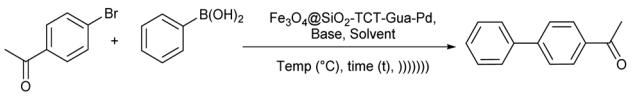

Scheme 2 Optimization of SMCR of 4-Bromoacetophenone and phenylboronic acid catalyzed by Fe_3O_4@SiO_2-TCT-Gua-Pd.

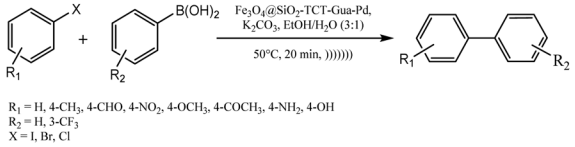

Scheme 3 Suzuki Miyaura cross coupling reaction using Fe_3O_4@SiO_2-TCT-Gua-Pd nanocatalyst.

Table 2 Suzuki Miyaura cross-coupling of aryl halides and aryl boronic acid catalyzed by Fe_3O_4@SiO_2-TCT-Gua-Pd[a]

Entry	Ar–X	Ar–$B(OH)_2$	Time (min)	Yield[b] (%)	TON/TOF (h^{-1})	Product
1		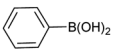	20	98	131/393	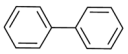
2		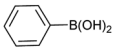	20	98	131/393	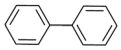
3		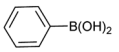	45	60	123/164	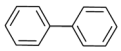
4	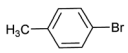	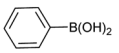	25	97	129/309	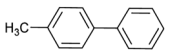
5	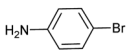	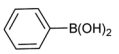	25	96	128/307	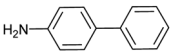
6	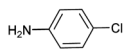	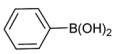	45	52	69/92	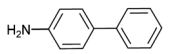
7	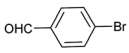	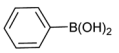	20	90	120/288	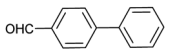
8	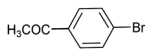	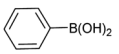	25	97	129/310	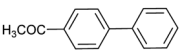
9	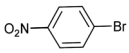	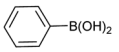	35	92	122/210	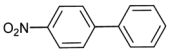
10	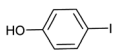	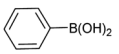	20	97	129/388	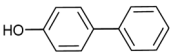
11	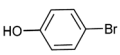	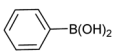	25	94	125/301	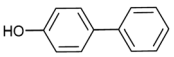
12	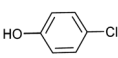	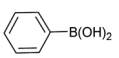	45	56	74/99	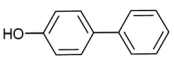
13	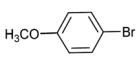	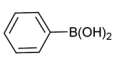	30	96	128/256	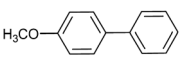
14	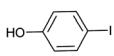		20	94	125/376	
15			25	97	129/310	
16			35	92	122/210	
17			35	88	117/201	
18[c]			45	60	80/106	

[a] Reaction condition: aryl halides (1.0 mmol), (1.2 mmol) aryl boronic acid, 3.0 mmol of K_2CO_3, Fe_3O_4@SiO_2-TCT-Gua-Pd (0.1 mol%), 50 °C under ultrasonication. [b] Isolated yield. [c] Reaction condition: aryl halide (1.0 mmol), (1.2 mmol) aryl boronic acid, 3.0 mmol of K_2CO_3, Fe_3O_4@SiO_2-TCT-Gua-Pd (0.1 mol%), 50 °C conventional heating.

times with high yield, as shown in Fig. 9. The activity dropped slightly in the 7th run. On the model reaction, a hot filtration test was performed to check for Pd leaching of the nanocatalyst. The reaction was carried out in the presence of the nanocatalyst until 70% conversion (after 10 min) and at that point, the nanocatalyst was magnetically separated at the reaction temperature. The reaction mixture was transferred to another vial, allowed the reaction to continue for 1 h, and was analyzed by GCMS, which showed that there was no further conversion. This showed that there has not been a discernible increase in the formation of the product. The filtrate was also analyzed for ICP-AES and the Pd content in the filtrate was negligible (<0.01 ppm). This demonstrated the fact that the observed catalysis was purely heterogeneous in nature, and Pd leaching was negligible. FTIR, XRD, and FESEM analyses were carried out for the recycled nanocatalyst, which revealed that the morphology remained unchanged, and the results are shown in Fig. 10. In order to demonstrate the applicability of Fe_3O_4@SiO_2-TCT-Gua-Pd nanocatalyst towards SMCR, a comparison with other reported heterogeneous palladium catalyst was done. As shown in Table 3, our catalyst system was compared with other reported catalysts and was found to be efficient with 98% yield within shorter time periods at low catalyst loading and compatible with the environment.

3.4 Synthetic scope of the nanocatalyst

In addition to SMCR, the scope of the prepared Fe_3O_4@SiO_2-TCT-Gua-Pd nanocatalyst was also checked for Heck–Mizoroki

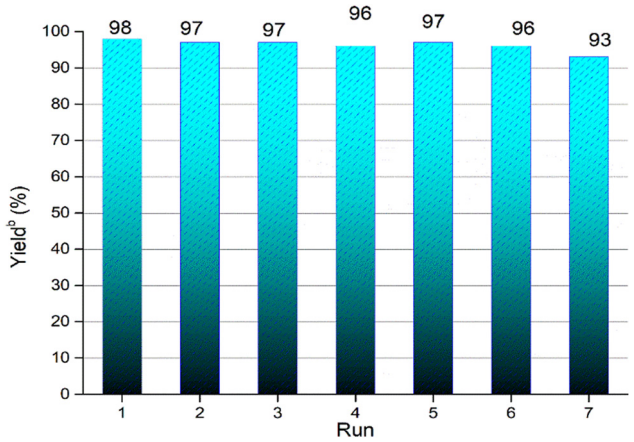

Fig. 9 Yields of biphenyl through Suzuki–Miyaura cross-coupling reaction catalyzed by Fe_3O_4@SiO_2-TCT-Gua-Pd nanocatalyst in different cycles. [a]Reaction condition: 1.0 mmol of 4-bromoacetophenone, (1.2 mmol) of phenyl boronic acid, 3.0 mmol K_2CO_3, Fe_3O_4@ SiO_2-TCT-Gua-Pd (0.1 mol%), 50 °C under ultrasonication b Isolated yields.

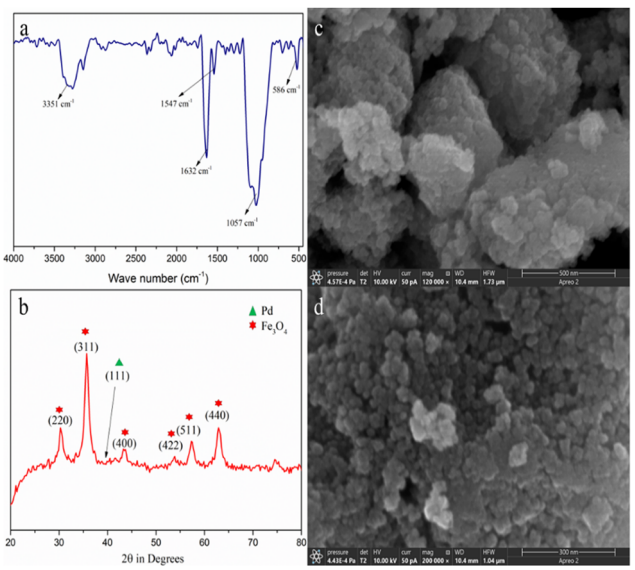

Fig. 10 (a) FTIR spectrum (b) XRD pattern (c) and (d) FESEM images at different magnifications of Fe_3O_4@ SiO_2-TCT-Gua-Pd nanocatalyst after the 7th cycle of SMC reaction.

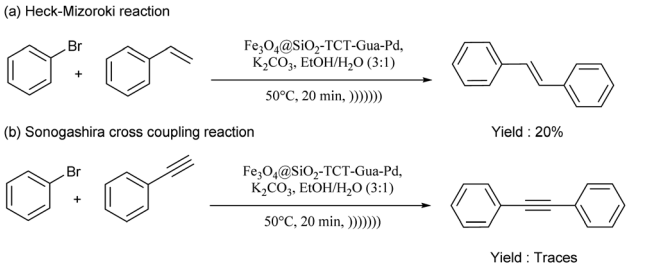

Scheme 4 Scope of catalyst in other cross coupling reactions.

(Scheme 4a) and Sonogashira cross-coupling reactions (Scheme 4b). Under the optimized conditions, the reactions did not give appreciable yields.

4. Conclusions

In conclusion, successful palladium doping has been achieved on the prepared magnetic Fe_3O_4@SiO_2-TCT-Gua nanocomposite using a simple method. Characterization of the Fe_3O_4@ SiO_2-TCT-Gua-Pd catalyst was performed with various analytical techniques, and all the analyses confirmed the successful preparation of the nanocatalyst. The catalytic activity of Fe_3O_4@SiO_2-TCT-Gua-Pd was evaluated in ultrasound-mediated Suzuki–Miyaura cross-coupling reaction, and it was noted that aryl halides were efficiently converted to desired biphenyls with very good yields and high turnover frequency within 20 min. Further, the reusability test of Fe_3O_4@SiO_2-TCT-Gua-Pd indicated that it could be reused for at least 6 consecutive runs without a loss in the reaction yields.

Author contributions

Sumanth Hegde: conceptualization, investigation, formal analysis, writing-original draft. Aatika Nizam: conceptualization, data curation, validation, resources, formal analysis, project administration, supervision, writing-original draft. Ajesh Vijayan: resources, formal analysis, data curation, writing-original draft. Ramesh B. Dateer: data curation, formal analysis, validation, writing original draft. Suresh Babu Naidu Krishna: data

Table 3 Comparison of Fe_3O_4@SiO_2-TCT-Gua-Pd with other catalysts towards Suzuki Miyaura reaction

Entry	Catalyst (mol%)	Conditions	Yield[a] (%)	Ref.
1	**Fe_3O_4@SiO_2-TCT-Gua-Pd (0.1)**	**K_2CO_3, H_2O/EtOH, 20 min**	**98**	**Current work**
2	Fe_3O_4/DAG/Pd (0.2)	K_2CO_3, H_2O/EtOH, 40 min, rt	98	H. Veisi *et al.*[46]
3	PS-Pd(II)-furfural (0.5)	K_2CO_3, H_2O/DMF, 80 °C, 5 h	98	S.M.Islam *et al.*[47]
4	Pd/Fe_3O_4/r-GO (0.36)	K_2CO_3, H_2O, 80 °C, 25 min	97	S. J. Hoseini *et al.*[48]
5	Fe_3O_4/o-PDA-Pd (0.2)	K_2CO_3, $NaBH_4$, DCM, rt, 45 min	97	A. Maleki *et al.*[49]
6	Fe_3O_4@SiO_2-TCT-GA-Pd (0) (0.12)	K_2CO_3, H_2O/EtOH, 50 °C, 1.5 h	95	H. Eslahi *et al.*[50]
7	Fe_3O_4/Ethyl-CN/Pd (0.2)	K_2CO_3, H_2O/EtOH, rt, 1 h	96	B. A. Khakiani *et al.*[51]
8	Fe_3O_4@SiO_2/isoniazide/Pd (0.2)	K_2CO_3, H_2O/EtOH, 25 °C, 1.5 h	96	F. Heidari *et al.*[52]
9	Fe_3O_4@SiO_2-Pd (0.03)	CaO, H_2O/EtOH, 80 °C, 30 min	90	A. Khazaei *et al.*[53]
10	Fe_3O_4@SiNSB-Pd (0.017)	K_2CO_3, H_2O/EtOH, 80 °C, 3 h	86	Md. Lutfor *et al.*[54]
11	Pd/CSP (0.2)	Et_3N, H_2O, 90 °C, 3.5 h	95	C. Putta *et al.*[55]

[a] Isolated yields.

curation, resources, formal analysis, validation, writing-review and editing.

Conflicts of interest

The authors declare that they have no known competing financial interests or personal relationships that could have appeared to influence the work reported in this paper.

Acknowledgements

The authors would like to acknowledge the support from CHRIST (Deemed to be University) for the research project funding (MRP #MRPDSC-1722) and laboratory facility for conducting experiments. Furthermore, the authors acknowledge the support of the Sophisticated Test and Instrumentation Centre (STIC), Cochin, India for HRTEM, and Gandhigram Rural Institute (Deemed to be University) for recording the NMR and TGA for the samples. KSBN would like to thank Durban University of Technology (DUT), South Africa, for a research fellowship and Director, Institute for Water and Wastewater Technology, DUT, South Africa.

References

1 B. B. Shaik, P. Seboletswe, S. B. Mohite, N. K. Katari, M. D. Bala, R. Karpoormath and P. Singh, *ChemistrySelect*, 2022, **7**(5), e202103701.
2 M. Arunachalapandi and S. M. Roopan, *High Energy Chem.*, 2022, **56**(2), 73–90.
3 R. J. Bull, D. A. Reckhow, X. Li, A. R. Humpage, C. Joll and S. E. Hrudey, *Toxicology*, 2011, **286**(1), 1–19.
4 P. Bałczewski, E. Kowalska, J. Skalik, M. Koprowski, K. Owsianik and E. Różycka-Sokołowska, *Ultrason. Sonochem.*, 2019, **58**, 104640.
5 M. P. Rayaroth, U. K. Aravind and C. T. Aravindakumar, *Ultrason. Sonochem.*, 2018, **40**, 213–220.
6 P. Poddar, J. Gass, D. J. Rebar, S. Srinath, H. Srikanth, S. A. Morrison and E. E. Carpenter, *J. Magn. Magn. Mater.*, 2006, **307**(2), 227–231.
7 C. W. Lim and I. S. Lee, *Nano Today*, 2010, **5**(5), 412–434.
8 M. Mohammadi, A. Ghorbani-Choghamarani and N. Hussain–Khil, *J. Phys. Chem. Solids*, 2023, **177**, 111300.
9 M. J. Madhura, A. S. Jeevan Chakravarthy, S. Hariprasad and V. Gayathri, *Catal. Lett.*, 2023, **153**(4), 1141–1149.
10 S. R. Chemler, D. Trauner and S. J. Danishefsky, *Angew. Chem., Int. Ed.*, 2001, **40**(24), 4544–4568.
11 M. Akkoç, N. Buğday, S. Altın, N. Kiraz, S. Yaşar and İ. Özdemir, *J. Organomet. Chem.*, 2021, **943**, 121823.
12 M. Akkoç, N. Buğday, S. Altın and S. Yaşar, *Appl. Organomet. Chem.*, 2021, **35**, e6233.
13 P. Devendar, R.-Y. Qu, W.-M. Kang, B. He and G.-F. Yang, *J. Agric. Food Chem.*, 2018, **66**(34), 8914–8934.
14 M. Farhang, A. R. Akbarzadeh, M. Rabbani and A. M. Ghadiri, *Polyhedron*, 2022, **227**, 116124.
15 P.-L. T. Boudreault, M. A. Esteruelas, E. Mora, E. Oñate and J.-Y. Tsai, *Organometallics*, 2019, **38**(15), 2883–2887.
16 M. Mohammadi, A. Ghorbani-Choghamarani and S. M. Ramish, *J. Mol. Struct.*, 2023, **1292**, 136115.
17 H. Maati, O. Amadine, Y. Essamlali, I. Ayouch, H. Mahi, K. Abdelouahdi and M. Zahouily, *J. Mol. Struct.*, 2023, **1294**(2), 136347.
18 M. Akkoç, N. Buğday, S. Altın, İ. Özdemir and S. Yaşar, *Catal. Lett.*, 2022, **152**, 1621–1638.
19 U. Veerabagu, Z. Chen, J. Xiang, Z. Chen, M. Liu, H. Xia and F. Lu, *J. Environ. Chem. Eng.*, 2021, **9**(3), 105246.
20 N. Buğday, S. Altın and S. Yaşar, *Appl. Organomet. Chem.*, 2021, **35**(11), e6403.
21 N. Shang, C. Feng, H. Zhang, S. Gao, R. Tang, C. Wang and Z. Wang, *Catal. Commun.*, 2013, **40**, 111–115.
22 L. Chen, Z. Gao and Y. Li, *Catal. Today*, 2015, **245**, 122–128.
23 M. Mohammadi, M. Khodamorady, B. Tahmasbi, K. Bahrami and A. Ghorbani-Choghamarani, *J. Ind. Eng. Chem.*, 2021, **97**, 1–78.
24 M. Beiranvand, D. Habibi and H. Khodakarami, *ACS Omega*, 2023, **8**(29), 25924–25937.
25 C. Li, H. Lv, K. Yang and X. Zhang, *ACS Appl. Mater. Interfaces*, 2023, **15**(29), 35052–35061.
26 Z. Esam, M. Akhavan, A. Bekhradnia, M. Mohammadi and S. Tourani, *Catal. Lett.*, 2020, **150**(11), 3112–3131.
27 M. Kumari, Y. Jain, P. Yadav, H. Laddha and R. Gupta, *Catal. Lett.*, 2019, **149**(8), 2180–2194.
28 R. V. Hegde, T.-G. Ong, R. Ambre, A. H. Jadhav, S. A. Patil and R. B. Dateer, *Catal. Lett.*, 2021, **151**(5), 1397–1405.
29 M. Kazemi and M. Mohammadi, *Appl. Organomet. Chem.*, 2020, **34**, e5400.
30 M. Boroujerdian, S. Rahimi, S. M. Nezhad, S. A. Pourmousavi, E. N. Zare, F. Salimi and H. Daneshgar, *Environ. Res.*, 2023, **236**, 116708.
31 M. Kazemi Miraki, M. Arefi, E. Yazdani, S. Abbasi, M. Karimi, K. Azizi and A. Heydari, *ChemistrySelect*, 2016, **1**(19), 6328.
32 G. Halligudra, C. C. Paramesh, R. Mudike, M. Ningegowda, D. Rangappa and P. D. Shivaramu, *ACS Omega*, 2021, **6**(50), 34416.
33 E. C. Santos, T. C. Dos Santos, R. B. Guimarães, L. Ishida, R. S. Freitas and C. M. Ronconi, *RSC Adv.*, 2015, **5**(59), 48031–48038.
34 I. R. Baxendale, C. M. Griffiths-Jones, S. V. Ley and G. K. Tranmer, *Chem. – Eur. J.*, 2006, **12**(16), 4407–4416.
35 W. Zhang, J. Bu, L. Wang, P. Li and H. Li, *Org. Chem. Front.*, 2021, **8**(18), 5045–5051.
36 C. E. Domini, G. F. Silbestri, B. Fernández Band and A. B. Chopa, *Ultrason. Sonochem.*, 2012, **19**(3), 410–414.
37 B. Datta, M. B. Madhusudana Reddy and M. A. Pasha, *Synth. Commun.*, 2011, **41**(15), 2331–2336.
38 D. Luo, G. Wu, H. Yang, M. Liu, W. Gao, X. Huang, J. Chen and H. Wu, *Ultrason. Sonochem.*, 2015, **27**, 192–199.
39 S. V. Sancheti and P. R. Gogate, *Ultrason. Sonochem.*, 2018, **40**, 30–39.

40 B. Datta and M. A. Pasha, *Ultrason. Sonochem.*, 2012, **19**(4), 725–728.
41 M. Mishra, A. Nizam, K. J. Jomon and K. Tadaparthi, *Russ. J. Org. Chem.*, 2019, **55**(12), 1925–1928.
42 H. Veisi, T. Ozturk, B. Karmakar, T. Tamoradi and S. Hemmati, *Carbohydr. Polym.*, 2020, **235**, 115966.
43 G. Cravotto and P. Cintas, *Chem. Soc. Rev.*, 2006, **35**(2), 180–196.
44 L. Hou, H. Zhang and X. Xue, *Sep. Purif. Technol.*, 2012, **84**, 147–152.
45 L. C. Hagenson, S. D. Naik and L. K. Doraiswamy, *Chem. Eng. Sci.*, 1994, **49**(24), 4787–4800.
46 H. Veisi, J. Gholami, H. Ueda, P. Mohammadi and M. Noroozi, *J. Mol. Catal. A: Chem.*, 2015, **396**, 216–223.
47 S. M. Islam, N. Salam, P. Mondal and A. S. Roy, *J. Mol. Catal. A: Chem.*, 2013, **366**, 321–332.
48 S. J. Hoseini, V. Heidari and H. Nasrabadi, *J. Mol. Catal. A: Chem.*, 2015, **396**, 90–95.
49 A. Maleki, R. Taheri-Ledari, R. Ghalavand and R. Firouzi-Haji, *J. Phys. Chem. Solids*, 2020, **136**, 109200.
50 H. Eslahi, A. R. Sardarian and M. Esmaeilpour, *Appl. Organomet. Chem.*, 2021, **35**(7), 1–21.
51 B. Abbas Khakiani, K. Pourshamsian and H. Veisi, *Appl. Organomet. Chem.*, 2015, **29**(5), 259–265.
52 F. Heidari, M. Hekmati and H. Veisi, *J. Colloid Interface Sci.*, 2017, **501**, 175–184.
53 A. Khazaei, M. Khazaei and M. Nasrollahzadeh, *Tetrahedron*, 2017, **73**(38), 5624–5633.
54 M. L. Rahman, M. S. Sarjadi, M. S. Akhter, J. J. Hannan and S. M. Sarkar, *Arabian J. Chem.*, 2022, **15**(8), 103983.
55 C. B. Putta and S. Ghosh, *Adv. Synth. Catal.*, 2011, **353**(11–12), 1889–1896.

